Journal of Catalysis 345 (2017) 87–95

Contents lists available at ScienceDirect

Journal of Catalysis

journal homepage: www.elsevier.com/locate/jcat

Novel photocatalytic activity of Cu@V co-doped TiO_2/PU for CO_2 reduction with H_2O vapor to produce solar fuels under visible light

Thanh-Dong Pham, Byeong-Kyu Lee *

Department of Civil and Environmental Engineering, University of Ulsan, Daehakro 93, Namgu, Ulsan 680-749, Republic of Korea

ARTICLE INFO

Article history:
Received 27 September 2016
Revised 29 October 2016
Accepted 31 October 2016

Keywords:
Co-doping
Oxygen vacancy
Ti^{3+} formation
CO_2 reduction
Solar fuels

ABSTRACT

In this study, Cu and V co-doped TiO_2 deposited on polyurethane (Cu@V-TiO_2/PU) was synthesized as a catalyst for the reduction of CO_2 with H_2O vapor to preferentially produce CH_4 as a valuable solar fuel under visible light. The Cu and V dopants defected into the TiO_2 lattice, leading to the formation of Ti^{3+} and oxygen vacancies in the lattice. The Ti^{3+} formed in the doped TiO_2 lattice created an intermediate band between the valence band and the conduction band of TiO_2, leading to an increase in the electron–hole pair separation efficiency of TiO_2. The oxygen vacancies existing on the surface of the photocatalyst could induce new adsorption sites to adsorb CO_2. The generated electrons and holes reacted with the adsorbed CO_2 and with H_2O vapor to produce CO and primarily CH_4. Therefore, the Cu@V-TiO_2/PU photocatalysts successfully utilized visible light as the energy source and H_2O vapor as a reductant to reduce CO_2 to CO and CH_4. The Cu@V-TiO_2/PU photocatalysts also supplied sufficient electrons and holes for the selective reduction of CO_2 to CH_4 rather than CO. The 2Cu@4V-TiO_2/PU photocatalyst, with Cu/TiO_2 and V/TiO_2 ratios of 2 and 4 wt.%, respectively, exhibited the highest photocatalytic activity for CO_2 conversion into solar fuels. The production rates of CH_4 and CO produced from the CO_2 reduction by the 2Cu@4V-TiO_2/PU photocatalyst under visible light were 933 and 588 μmol g^{-1} cat. h^{-1}, respectively.

1. Introduction

Carbon dioxide (CO_2) emission has become a major cause of the greenhouse effect, leading to global warming and climate change [1,2]. Atmospheric concentrations of CO_2 have greatly risen since the Industrial Revolution and the current rate of ambient concentration increase is alarming. Therefore, many studies have been conducted to reduce CO_2 concentrations [1–5]. The utilization of solar energy for the conversion of CO_2 into valuable fuels is one promising technology, which not only mitigates the increasing level of CO_2 in the environment but also provides alternative fuels simultaneously to overcome the energy crisis [6]. Since Inoue et al.'s pioneering work demonstrating the photocatalytic reduction of CO_2 to organic compounds, research on the photocatalytic conversion of CO_2 has received increasing attention [2,7–10]. The photocatalytic reduction utilizes ultraviolet (UV) and/or visible light as the excitation source for photocatalysis to generate electron–hole pairs, which can reduce CO_2 with H_2O adsorbed onto the photocatalyst surface to form valuable products such as carbon monoxide (CO), methane (CH_4), methanol (CH_3OH), formaldehyde (HCHO), and formic acid (HCOOH), depending upon the available electrons [4]. Among the various photocatalysts, titanium dioxide (TiO_2), which is a cheap, nontoxic, and abundant semiconductor and resistant to photocorrosion, has been most widely used. However, the major challenges of the TiO_2 photocatalyst are its wide band gap (~3.2 eV for anatase and 3.0 eV for rutile) and fast recombination of photogenerated electrons and holes, resulting in low efficiency of photocatalysis and limited utilization of solar energy [8]. The photocatalytic conversion of CO_2 by the TiO_2 photocatalyst is also limited because of its poor adsorption capability for CO_2 [11].

For improving the photocatalytic activity of TiO_2 by enhancing the visible response and reducing the recombination rate of the photogenerated electrons and holes, many strategies have been proposed, including the loading of metals, metal oxides, and doping nonmetal ions [2,8,11–16]. Xiong et al. reported that modification of TiO_2 with metal elements reduced the recombination of the photogenerated electron–hole pairs and extended the spectral response from UV to the visible area, simultaneously [17]. In our previous studies, Cu and V were individually used as metal elements to enhance the photocatalytic activity of TiO_2 for air purification purposes [14,15,18,19]. The obtained results indicated that these metals acted as dopants (incorporated into the TiO_2 lattice) and supporters (existing in the form of metals or metal oxides

* Corresponding author. Fax: +82 52 259 2629.
E-mail address: bklee@ulsan.ac.kr (B.-K. Lee).

http://dx.doi.org/10.1016/j.jcat.2016.10.030
0021-9517/

distributed on the surface of the TiO_2 layer) to enhance the photocatalytic activity of the TiO_2 photocatalyst. Thus, the synthesized Cu and V single-doped TiO_2 exhibited very high photocatalytic activity, even under visible light irradiation. More recently, numerous studies have doped TiO_2 with two different dopants (co-doping) to synergistically improve the photocatalytic activity of the photocatalyst [12,13,20–22]. Therefore, in this study, we combine Cu and V as co-dopants to synergistically enhance the photocatalytic activity of TiO_2 for CO_2 conversion to produce valuable fuels under visible light. In addition, the co-doping is expected to increase defects or disorders in the TiO_2 lattice. Paulino et al. reported that the disorders in the TiO_2 lattice influenced CO_2 adsorption, activation, and dissociation processes [2]. Rodriguez et al. also reported that the presence of defects on the TiO_2 surface induced the formation of new adsorption sites to capture CO_2, after which the electrons stored in the oxygen vacancies were spontaneously transferred to CO_2, which in turn was finally reduced [23]. Therefore, the co-doping is also expected to increase disorder in the TiO_2 lattice, leading to an increase in CO_2 adsorption or photocatalytic reduction of CO_2. In our previous studies, we investigated the use of porous polyurethane (PU), a honeycomb structure material, as a substrate to immobilize the Cu-doped TiO_2 and V-doped TiO_2 photocatalysts [14,15,19]. This synthesized structure not only overcame the disadvantages faced by the powder photocatalysts but also increased the adsorption ability of the photocatalysts. Therefore, in this study, we again used PU as the substrate to immobilize Cu@V co-doped TiO_2 (Cu@V-TiO_2/PU) in order to enhance the surface area and CO_2 adsorption capacity and thereby attain high photocatalytic activity and CO_2 adsorption capacity to overcome all the drawbacks of CO_2 conversion by photocatalysis.

2. Experimental

2.1. Photocatalyst preparation

We used a mixture of toluene, toluene-2,4-diisocyanate, and anhydrous triethylamine to activate pristine PU to introduce isocyanate groups onto its surface [14,15,19,24]. Titanium tetraisopropoxide and γ-aminopropyltriethoxysilane were used as precursors for synthesis of amino titanosiloxane, which contains amine groups (NH_2). The isocyanated PU was immersed in the synthesized amino titanosiloxane solution to promote the reaction between the isocyanate groups of the isocyanated PU and the NH_2 groups of the amino titanosiloxane to form urea bonds, which fixed the titanosiloxane on the PU surface. To synthesize Cu@V co-doped TiO_2/PU, a mixture of 0.1 M $Cu(NO_3)_2$ and 0.1 M NH_4VO_3 solution was added to the titanosiloxane fixed on PU. The obtained material was cleaned by a 1 M oxalic acid solution. Finally, the Cu@V-TiO_2/PU was irradiated and calcined by UV-C light (60 W) for 5 h under nitrogen at 200 °C. Seven different Cu@V-TiO_2/PU materials were synthesized by adjusting the added volumes of $Cu(NO_3)_2$ and NH_4VO_3 solutions. The TiO_2/PU ratio in the synthesized materials was approximately 20 wt.%. The total weight ratios of both dopants to TiO_2 (total Cu/TiO_2 and V/TiO_2 ratios) were fixed at 6 wt.%, and the weight ratio of each individual Cu and V dopant was varied between 0 and 6 wt.% at intervals of 1 wt.%. The synthesized materials were labeled *x*Cu@*y*V-TiO_2/PU, where *x* and *y* indicate the weight ratios of Cu/TiO_2 and V/TiO_2, respectively.

2.2. Photocatalyst characterization

The synthesized Cu@V-TiO_2/PU photocatalysts were analyzed by a Thermo Fisher K-Alpha X-ray Photoelectron Spectrometer (XPS) system. The obtained XPS spectra were fitted by Gaussian multipeak shapes to characterize the elemental states of copper, vanadium, and titanium in the synthesized photocatalysts. A Hitachi S4700 scanning electron microscope (SEM) was used to observe the surface morphology of the Cu@V-TiO_2/PU, which was coated with Pt before SEM analysis to increase the conductivity of the photocatalyst surface. A JEOL TEM-2010F system was used to obtain transmission electron microscopy (TEM) and high-resolution TEM (HR-TEM) images of the synthesized Cu@V-TiO_2/PU. The optical absorption ability of the shredded Cu@V-TiO_2/PU photocatalyst was characterized by an Evolution 300 spectrophotometer (UV-1700 Shimadzu). X-ray diffraction (XRD) spectra of the Cu@V-TiO_2/PU were obtained using a Bruker AXN model equipped with a Cu Kα radiation ($\lambda = 1.5418$ Å) source and operated at a scan rate of $0.02^\circ\ s^{-1}$ over the 2θ range 10–80°.

2.3. Conversion experiments

Photocatalytic reduction of CO_2 with H_2O vapor was conducted by a continuous system comprising a gas generator, reaction chamber, and analyzer. The gas generator consisted of a cylinder of CO_2 gas (99.99%), flow rate meters, and a humidifier. The reaction chamber was a dark cover cask (50 × 25 × 50 cm) containing two white light bulbs (EFTR 20EX-D, Kumho Co., Ltd.) and a reactor (15 × 4 × 2 cm), the top and bottom parts of which were made of quartz to allow easy passage of visible light ($400 < \lambda < 700$ nm). The reactor was placed in the center of the reaction chamber. Two 20 W white bulbs were placed at the top and the bottom of the reaction chamber to generate visible light in the range 400–700 nm with a power density of 0.05 W/cm^2 for the photocatalysis. The dark and visible light conditions for photocatalysis were achieved by turning the bulbs off and on, respectively. Before the photocatalytic conversion experiments, the reactor containing 2 g (36 cm^3) of the synthesized porous Cu@V-TiO_2/PU was purged three times with high-purity CO_2 gas. Then 50 mL/min CO_2 that had been passed through water (303 K) was admitted to the reactor. Thus, the residence time of CO_2 in the reactor was 144 s and the space velocity, calculated by dividing the volumetric flow by the reactor volume, was 25 h^{-1}. The reactor temperature was constant at 32 °C during the conversion experiments. To determine gaseous products, a 100 μL sample was automatically injected into the GC system, which consisted of a Varian CP-3800 gas chromatograph (GC) equipped with a methanizer and a flame ionization detector using a packed column (Porapak Q 80/100 2 × 2 mm) at intervals of 20 min. The reaction start time ($t_0 = 0$) was assumed to be the time when the CO_2 gas stream containing H_2O was admitted to the reactor. The production rate was calculated based on the total weight of synthesized catalyst (2 g).

3. Results and discussion

3.1. Material characteristics

3.1.1. Surface morphology and dopant states

Fig. 1 shows the SEM and elemental mapping of Ti, Cu, and V in the selected areas in the SEM images of the synthesized materials. In the TiO_2/PU, TiO_2 was smoothly immobilized on the PU surface as a thin layer (Fig. 1A). The surfaces of the Cu-TiO_2/PU, V-TiO_2/PU, and Cu@V-TiO_2/PU materials were rougher than that of TiO_2/PU due to the presence of both Cu and V on the metal-doped photocatalysts (Fig. 1B–D). High-resolution XPS spectra with Gaussian multipeak shapes of Cu2$p_{3/2}$ and V2$p_{3/2}$ peaks were obtained to indicate the elemental states of copper and vanadium in the synthesized Cu@V-TiO_2/PU (Fig. 2). The XPS spectra show that the Cu2$p_{3/2}$ peaks consist of two different peaks at 932.18 and 933.48 eV, corresponding to the binding energies of Cu2$p_{3/2}$ in the Cu^+ and Cu^{2+} states, respectively [25,26]. The Cu^+ and Cu^{2+} exist

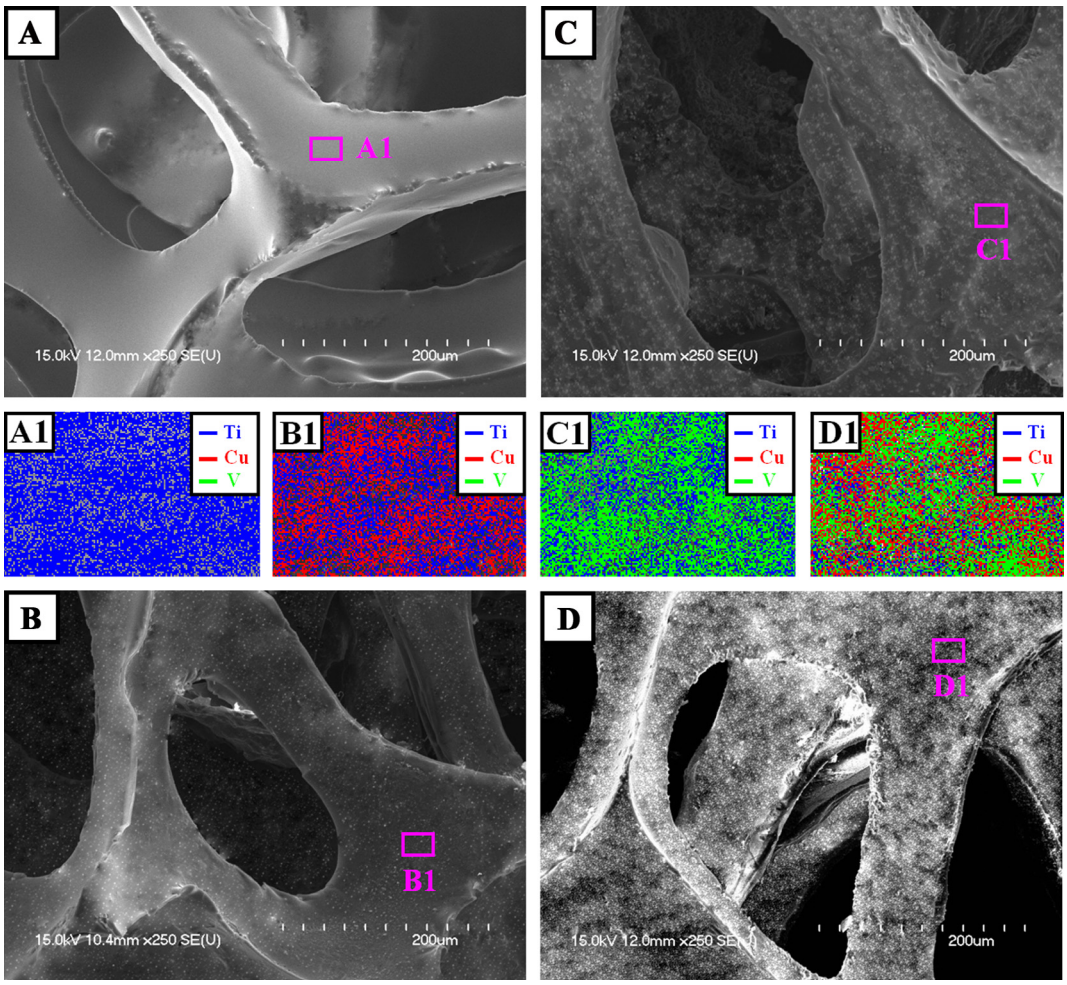

Fig. 1. SEM and elemental mapping of selected areas in SEM images of TiO_2/PU (A), 6Cu-TiO_2/PU (B), 6V-TiO_2/PU (C), and 3Cu@V-TiO_2/PU (D).

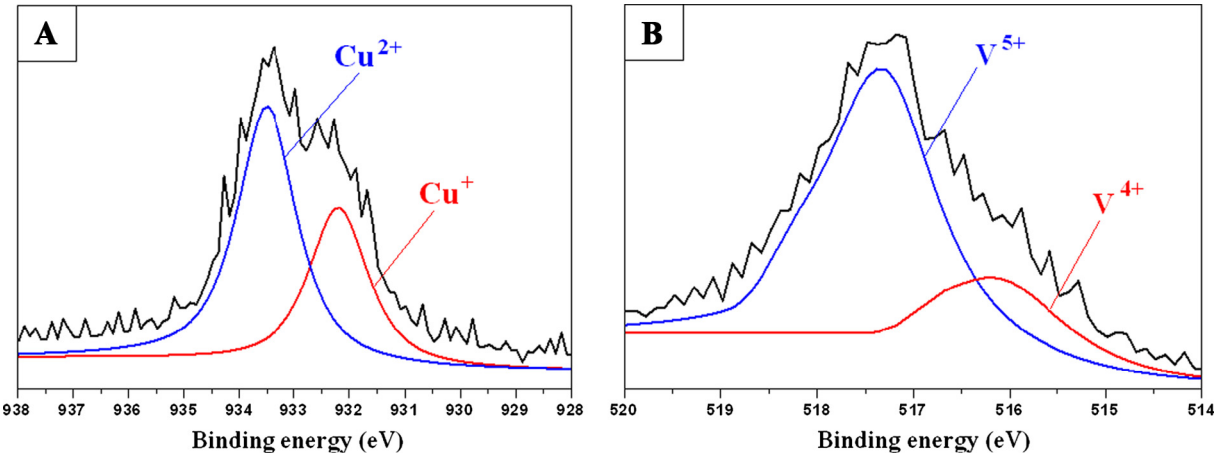

Fig. 2. XPS spectra of Cu2$p_{3/2}$ (A) and V2$p_{3/2}$ (B) in 3Cu@3V-TiO_2/PU.

in the form of either dopants (incorporated into the TiO_2 lattice) or Cu_2O and CuO oxides (distributed on the surface of the TiO_2 layer) [14,18,26,27]. The XPS spectra also show that the V2$p_{3/2}$ peaks consisted of two different peaks, observed at 516.0 and 517.4 eV, which were attributed to the binding energies of V2$p_{3/2}$ in the V^{4+} and V^{5+} states, respectively [28,29]. The V^{5+} state of vanadium corresponded to the state of V_2O_5 oxide distributed on the TiO_2 surface [15,28–30]. The V^{4+} ions exist as dopants incorporated into the TiO_2 lattice by substitutional replacement of the Ti^{4+} ions to form a Ti—O—V bond [15,31,32]. The various formed particles, such as CuO and Cu_2O oxides on the surface of the Cu-TiO_2/PU, V_2O_5 on the surface of the V-TiO_2/PU, and CuO, Cu_2O, and V_2O_5 on the surface of the Cu@V-TiO_2/PU, increased the roughness and hence the surface area of the metal-doped TiO_2 photocatalysts. Table 1 indi-

Table 1
Ti^{3+}/Ti^{4+} ratios, surface areas, band gap energies, and production rates of the synthesized materials.

	Ti^{3+}/Ti^{4+} ratios (%)	Surface areas (m^2/g)	Band gap energy (eV)	Production rates ($\mu mol\ g^{-1}\ cat.\ h^{-1}$)	
				CO	CH_4
TiO_2/PU	0	110.6	3.20	0	0
6Cu-TiO_2/PU	25.4	166.3	2.85	431	772
5Cu@1V-TiO_2/PU	30.9	190.9	2.80	464	803
4Cu@2V-TiO_2/PU	33.1	226.7	2.77	501	836
3Cu@3V-TiO_2/PU	34.4	232.2	2.70	577	902
2Cu@4V-TiO_2/PU	35.3	236.5	2.66	588	933
1Cu@5V-TiO_2/PU	33.9	221.3	2.73	531	865
6V-TiO_2/PU	30.1	192.6	2.83	453	794

cates that the BET surface areas of the metal-doped photocatalysts were much higher than that of the TiO_2/PU. Table 1 also shows that the surface areas of the co-doped photocatalysts were much higher than those of the single-doped photocatalysts. This was because the co-doping effect of Cu and V inhibited the aggregation of CuO, Cu_2O, and V_2O_5 particles formed on the surface of TiO_2 in the Cu@V-TiO_2/PU. Due to this inhibition, the formed particles were more uniformly distributed and their fractions were smaller than those in the single-doped photocatalysts [29]. Therefore, the surface areas of the Cu@V-TiO_2/PU photocatalysts were much higher than those of the Cu-TiO_2/PU and V-TiO_2/PU photocatalysts. The incorporation of Cu and V in the TiO_2 lattice also distorted the formation of the TiO_2 layer, which increased the surface areas of the synthesized co-doped photocatalysts. The optimal combination weight ratios of 2 wt.% Cu/TiO_2 and 4 wt.% V/TiO_2 led to the largest BET surface area of 236.5 (m^2/g) for 2Cu@4V-TiO_2/PU.

3.1.2. Microstructure and co-doping effects

Fig. 3 shows the XRD patterns of the synthesized TiO_2/PU, Cu-TiO_2/PU, V-TiO_2/PU, and Cu@V co-doped TiO_2/PU. The obtained results indicate that all the TiO_2 in the TiO_2/PU and V-TiO_2/PU existed in the anatase phase [29]. However, the XRD patterns of Cu-TiO_2/PU and Cu@V-TiO_2/PU shows additional peaks at 27.5° and 36.1°, corresponding to rutile peaks of TiO_2 (Fig. 3). Rutile peaks occurred due to the Cu dopants, which accelerated the anatase–rutile phase transformation or the formation of the rutile phase in the TiO_2 [33,34]. In addition, the (101) anatase peak of the TiO_2 in the XRD patterns of both single- and co-doped materials was more left-shifted and broader than that in the TiO_2/PU. This was due to the metal dopants incorporated into the crystal structure of TiO_2, leading to distortions in the crystal lattice [35–38]. The Cu and V dopants defected into and substituted for the Ti^{4+} ions in the TiO_2 lattice by forming Cu—O—Ti and Ti—O—V bonds, respectively [39,40]. This substitution led to the formation of Ti^{3+} ions or oxygen vacancies in the metal-doped TiO_2/PU materials [41,42]. The obtained XPS results of the doped TiO_2 materials confirmed the existence of Ti^{3+} in the TiO_2 lattice (Fig. 4). The calculated Ti^{3+}/Ti^{4+} ratios, which are proportional to the ratios (area under the Ti^{3+} peak)/(area under the Ti^{4+} peak) in the obtained XPS spectra of the synthesized metal-doped TiO_2, are also listed in Table 1. The obtained results show that the Ti^{3+}/Ti^{4+} ratio in the V single-doped photocatalyst (6V-TiO_2/PU) was higher than that in the Cu single-doped photocatalyst (6Cu-TiO_2/PU). This was because the ionic radius of V^{4+} (0.72 Å) is closer to that of Ti^{4+} (0.74 Å) than is that of Cu^{2+} (0.87 Å), and hence the V^{4+} was more effectively doped into the TiO_2 lattice than the Cu^{2+} was, which increased the oxygen vacancy (or formation of Ti^{3+}) in the V single-doped photocatalyst more than that in the Cu single-doped photocatalyst [31,32]. The Ti^{3+}/Ti^{4+} ratio in the Cu@V-TiO_2/PU co-doped photocatalyst was higher than that in either the Cu or V single-doped photocatalyst. This indicates that the Cu and V co-doping further enhanced the defects in the TiO_2 lattice, thus increasing the formation of oxygen vacancies or Ti^{3+} compared with the case of the single-doped with Cu and V. In the co-doped photocatalysts, when the V/TiO_2 ratio was increased to 4 wt.% (2Cu@4V-TiO_2/PU), the Ti^{3+}/Ti^{4+} ratio increased to a maximum of 35.3%, but then decreased slightly with further increase in the V/TiO_2 ratio. Therefore, the optimal combination weight ratio of 2 wt.% Cu/TiO_2 and 4 wt.% V/TiO_2 led to the most defects in the TiO_2 lattice.

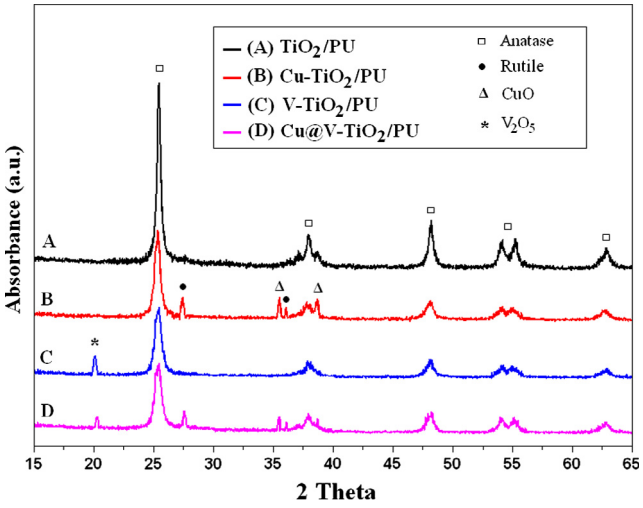

Fig. 3. XRD patterns of TiO_2/PU, Cu-TiO_2/PU, V-TiO_2/PU, and 3Cu@3V-TiO_2/PU.

3.1.3. Optical properties and band gap energy

The optical absorption spectra of the synthesized TiO_2/PU, Cu-TiO_2/PU, V-TiO_2/PU, and Cu@V-TiO_2/PU materials indicate that the synthesized TiO_2/PU inherited all the optical absorption properties of TiO_2, which only absorbs UV light with the absorption edge at ~370 nm (Fig. 5) [42,43]. However, the optical absorption of the twin-metal-doped TiO_2/PU materials was observed in both the UV and visible regions. The significant enhancement of the optical absorption in the visible region of the twin-metal-doped TiO_2/PU was due to the synergistic contribution of Cu and V dopants. The dopants defected into the TiO_2 lattice led to oxygen vacancies and the formation of Ti^{3+} in the TiO_2 lattice. The formed Ti^{3+} in the doped TiO_2 lattice created an intermediate band between the valence band and the conduction band of TiO_2, which increased the electron–hole pair separation efficiency of TiO_2 and the light absorption enhancement of the metal-doped TiO_2/PU [44]. The formed oxides (CuO, Cu_2O, and V_2O_5) distributed on the surface of the TiO_2 layer also combined with TiO_2 to create a suitable semiconductor–semiconductor system, which increased the electron transfer from the valence band to the conduction band

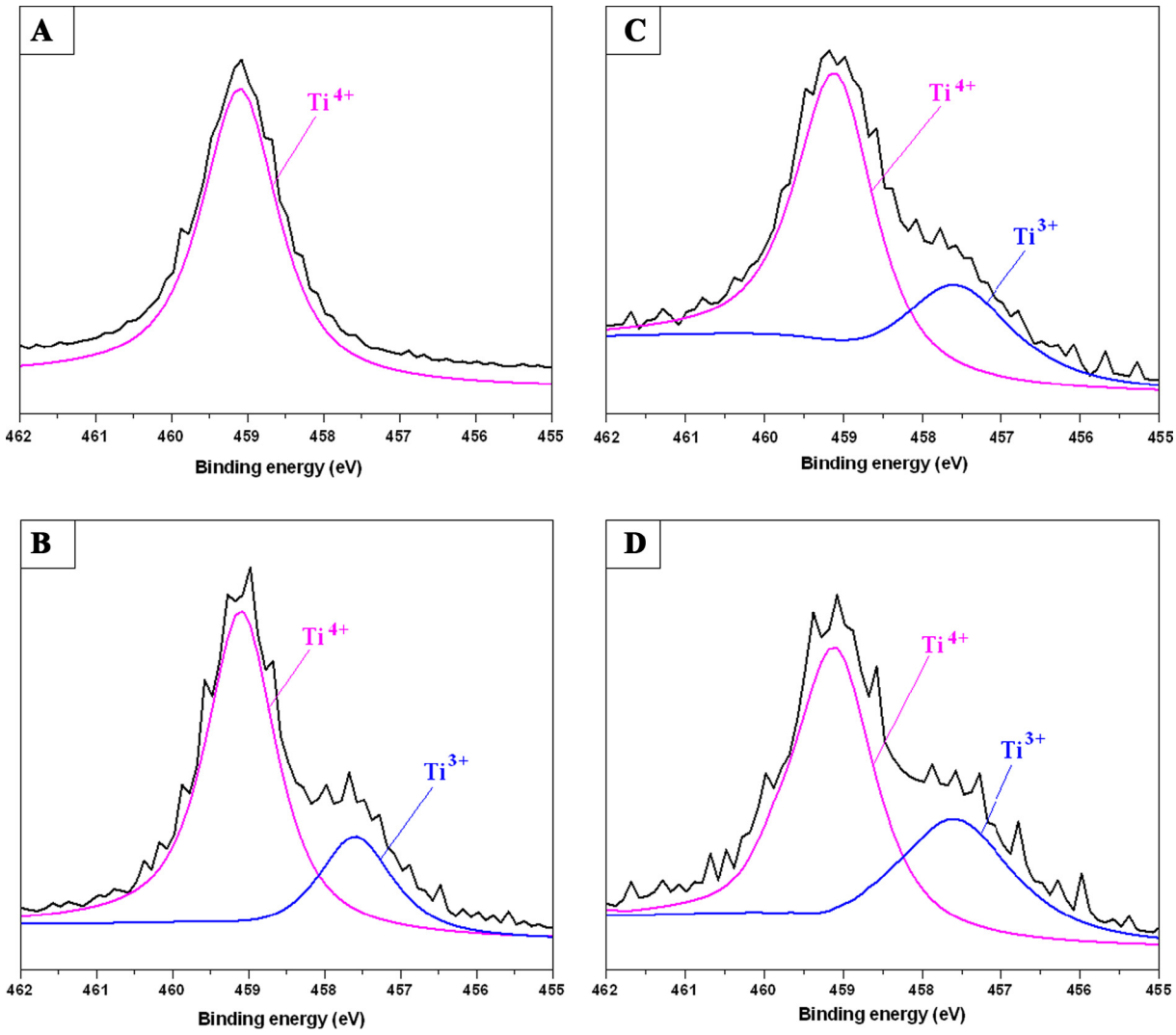

Fig. 4. XPS spectra of Ti2$p_{3/2}$ in TiO_2/PU (A), Cu-TiO_2/PU (B), V-TiO_2/PU (C), and 3Cu@3V-TiO_2/PU (D).

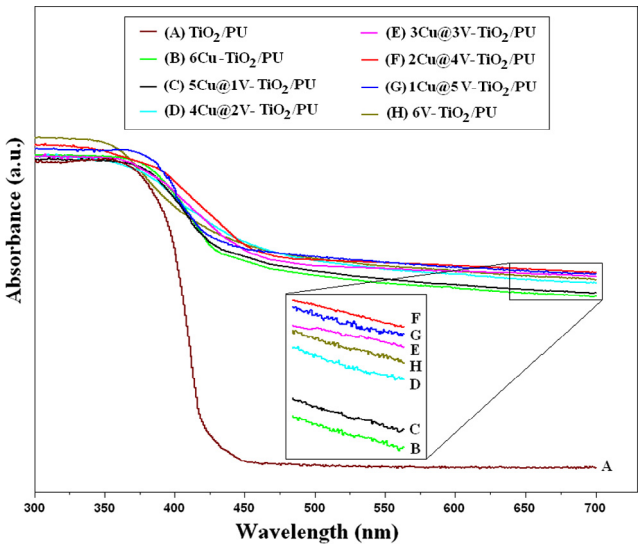

Fig. 5. UV–Vis absorption spectra of the synthesized TiO_2/PU and Cu@V-TiO_2/PU.

of TiO_2 and thereby enhanced the light absorption of the metal-doped TiO_2/PU [45]. The Cu and V co-doped TiO_2/PU photocatalysts inherited all the advantages of these individual single dopants to enhance their light absorption efficiency. The obtained results indicate that 2Cu@4V-TiO_2/PU, with Cu/TiO_2 and V/TiO_2 ratios of 2 and 4 wt.%, respectively, showed the greatest optical absorption ability in the visible light region. A Tauc plot combined with the Kubelka–Munk method was used to estimate the band gap energies of the synthesized photocatalysts [46,47]. In the Tauc plot, a linear fit was drawn from the transformed curves to the photon energy axis ($h\nu$). The energy value at the point of intersection of the line and the horizontal axis is the band gap energy of the material (Fig. 6). The obtained results indicate that the band gap energies of the synthesized Cu@V-TiO_2/PU were positively related to the Ti^{3+}/Ti^{4+} ratios (Table 1). As mentioned, the formed Ti^{3+} acted as an intermediate band between the valence band and the conduction band of TiO_2, thereby decreasing the band gap energy.

3.2. CO_2 reduction

3.2.1. Photocatalytic reduction mechanism

The experiments with CO_2 reduction by the synthesized photocatalysts were conducted under two different conditions. Under condition A, 50 mL/min CO_2 containing water was passed through the synthesized photocatalysts under dark conditions for 180 min and then irradiated with visible light for an additional 360 min.

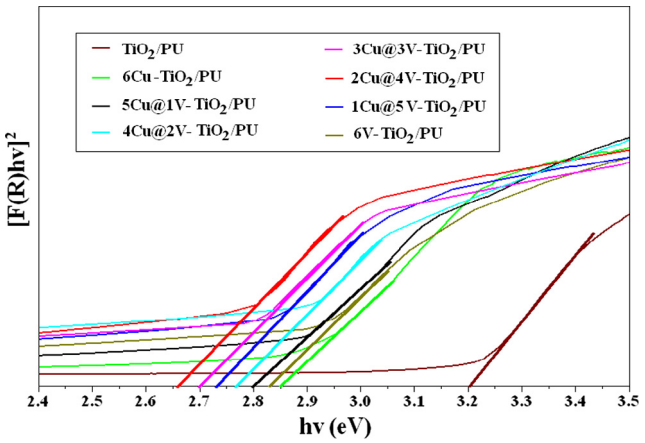

Fig. 6. Tauc plot of the synthesized TiO_2/PU and twin-metal-doped TiO_2/PU.

Under condition B, the visible light was immediately provided from the beginning of the reduction experiments (in the same CO_2 feed environment). The obtained results show that the synthesized TiO_2/PU and doped TiO_2/PU could not reduce CO_2 under dark conditions. Under visible light, the TiO_2/PU also did not exhibit any photocatalytic activity for CO_2 reduction; however, the doped TiO_2 photocatalysts reduced a certain amount of CO_2 into CO and CH_4. Fig. 7 shows the production rates for CO and CH_4 from the photocatalytic reduction of CO_2 by 3Cu@3V-TiO_2/PU. Under both conditions A and B, the production rates for CO and CH_4 gradually increased to a stable value after a certain irradiation time. However, in the early irradiation period, condition A produced CO and CH_4 at higher rates than condition B did (Fig. 7), because the photocatalysts adsorbed a certain amount of CO_2 and H_2O on their surfaces during the darkened period of condition A (preadsorption). As mentioned, the adsorption is the initial step for CO_2 conversion. Thus, the photocatalyst immediately reduced the adsorbed CO_2 to produce CO and CH_4 when it was irradiated with visible light after the darkened period. Under condition B, the photocatalysts were irradiated immediately with visible light when the CO_2 containing H_2O reached their surfaces. Therefore, the photocatalysts needed a certain time to adsorb CO_2 and H_2O, which slowed down the reduction. However, the adsorption of the CO_2 and H_2O on the photocatalyst gradually reached a balanced state because the CO_2 conversion experiment was conducted in an online system, in which 50 mL/min CO_2 containing water was continuously admitted to the photocatalyst. The adsorbate (CO_2 and H_2O) on the surface of each photocatalyst in the balanced state under the two experimented conditions was similar because in the balanced state the adsorption depends on the interactions between the photocatalyst and the adsorbate. Therefore, the CO_2 reduction rate and efficiency of the photocatalysts under the two provided conditions were similar after a certain irradiation time (when the "preadsorption" effects of condition A no longer existed). The Cu and V dopants defected into the TiO_2 lattice, leading to oxygen vacancies and the formation of Ti^{3+} in the lattice and thereby enhancing the separation of electron–hole pairs in the Cu@V-TiO_2/PU photocatalysts. The formed CuO, Cu_2O, and V_2O_5 oxides distributed on the TiO_2 surface acted as an electron sink (or electron transfer) to prevent recombination of the generated electrons and holes, also enhancing the electron–hole separation efficiency. Therefore, the synthesized Cu@V-TiO_2/PU photocatalysts generated a significant number of electron–hole pairs, even under visible light. The generated holes reacted with H_2O vapor to produce protons (H^+). The generated electrons reduced CO_2 to certain carbon radicals (reduced CO_2) such as $^{-}CO_2$ and C^* [48,49]. Finally, the reduced CO_2 reacted with the formed protons to produce CO and CH_4 (Fig. 8). The overall reactions to form CO and CH_4 are shown by the following equations:

$$\text{Metals-doped } TiO_2/PU \xrightarrow{\text{Visible light}} e^- + h^+, \quad \text{(E1)}$$

$$2H_2O + 4h^+ \rightarrow 4H^+ + O_2, \quad \text{(E2)}$$

$$CO_2 + 2H^+ + 2e^- \rightarrow CO + H_2O \quad (E^0_{redox} = -0.48\ V), \quad \text{(E3)}$$

$$CO_2 + 8H^+ + 8e^- \rightarrow CH_4 + 2H_2O \quad (E^0_{redox} = -0.24\ V), \quad \text{(E4)}$$

$$2H^+ \rightarrow H_2. \quad \text{(E5)}$$

Eqs. (E3) and (E4) show that 2 mol protons and 2 mol electrons are needed to generate 1 mol CO, whereas the formation of 1 mol CH_4 requires 8 mol protons and 8 mol electrons. In addition, a certain time was required to produce protons (via reaction (E2)). More time was also spent in diffusion of the produced protons to the carbon

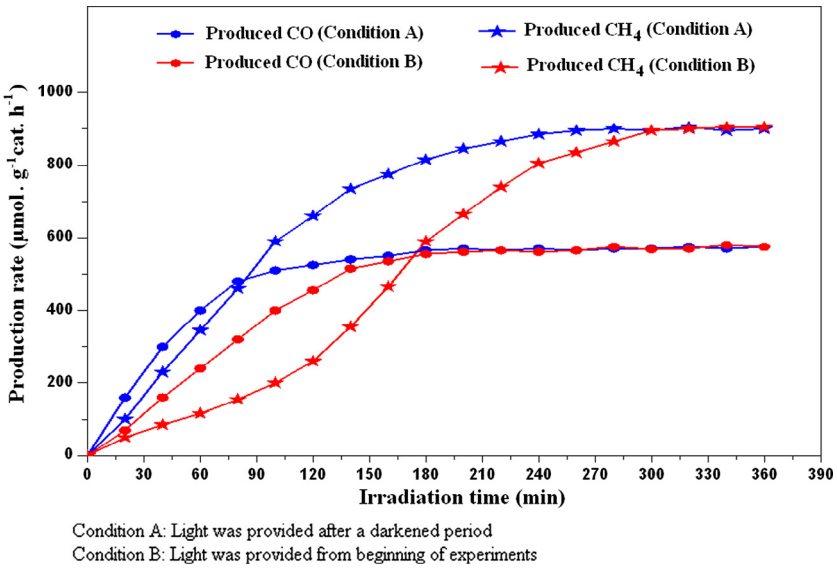

Fig. 7. Rates of CO and CH_4 production from the CO_2 photocatalytic reduction of 3Cu@3V-TiO_2/PU under different conditions.

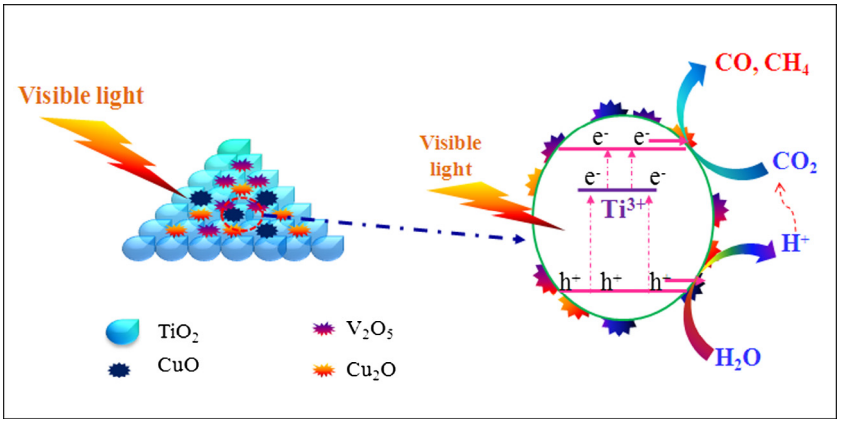

Fig. 8. Mechanism of CO_2 reduction by doped TiO_2 photocatalysts.

Table 2
Production rates of the photocatalytic conversion of CO_2.

Materials	Production rates (μmol g^{-1}cat. h^{-1})					CO_2 flow rate (mL/min)	Light sources and reductants	Ref.
	CH_4	CH_3OH	CO	H_2	O_2			
Cu@V-TiO_2/PU	935	–	588	30	2160	50	vis + Water vapor	The study
Cu-TiO_2	18	–	763	–	–	20	UV + H_2	[51]
Co-Fe	10	–	218	13	–	15	UV + NaCl + water	[53]
Au@CdS/TiO_2	41.6	–	0.6	18	109	–	vis + Water vapor	[54]
PO_4-C_3N_4	73	–	38	–	–	10	vis + $NaHCO_3$ solution	[55]
Au-TiO_2	–	13	1237	–	–	–	vis + H_2 gas	[52]
Pt^{2+}-Pt^0/TiO_2	64	–	55	394	290	200	UV + Water vapor	[17]
$CuCoO_4$	–	–	1150	245	–	–	vis + TEOA + Water	[56]
Ag/CFs	–	475	–	–	120	20	vis + Water	[57]
Pt/$LaPO_4$	220	–	–	40	–	–	UV + Water	[58]
Au-In/TiO_2	15	–	8982	–	–	–	UV + H_2	[59]
ZnO/g-C_3N_4	5	19	38.7	–	–	–	vis + Water	[60]

radicals. Therefore, in the early irradiation period, there was a small number of protons participating in reactions with CO_2. Thus, in this period, the CO was preferably produced rather than CH_4 due to lack of protons. However, after a certain irradiation time, the produced amount of CH_4 surpassed that of CO because the generation of CH_4 (E^0_{redox} = −0.24 V) is thermodynamically more feasible than that of CO (E^0_{redox} = −0.48 V) when there are sufficient protons and electrons. In the present study, the co-doping of Cu and V significantly enhanced the electron–hole separation of the TiO_2. Therefore, the synthesized materials generated a significant number of electrons and holes, even under visible light. The generated electrons were easily transferred to the photocatalyst surface by the CuO, Cu_2O, and V_2O_5 oxides (distributed on the TiO_2 surface) to react with protons, which were abundantly produced from the reduction of H_2O by the generated holes, leading to selective conversion of CO_2 into CH_4 rather than CO.

3.2.2. Optimizing doping contents

The rates of production of CO and CH_4 on synthesized Cu@V-TiO_2/PU with different doping ratios after approximately 5 h irradiation by visible light (when production rate was stable) are shown in Table 1. The obtained results indicate that the production rates of CO and CH_4 were positively related to the concentration of the formed Ti^{3+} (or oxygen vacancies) in the TiO_2 lattice. This is consistent with the possible roles of the Ti^{3+} and oxygen vacancies in the reduction of CO_2. The oxygen vacancies existing on the surface of the photocatalyst introduced new adsorption sites to adsorb CO_2. As mentioned in Section 3.2.1, the formation of Ti^{3+} enhanced the separation of electron–hole pairs of the photocatalysts and the generated electrons and holes participated in multiple reactions for the reduction of CO_2 by H_2O vapor [23,50]. Table 1 also shows that 2Cu@4V-TiO_2/PU exhibited the highest CO_2 reduction efficiency. The rates of CH_4 and CO production from the photocatalytic reduction of CO_2 with 2Cu@4V-TiO_2/PU under visible light were 933 and 588 (μmol g^{-1} cat. h^{-1}), respectively.

Table 2 show the rates of production for products of the photocatalytic reduction of CO_2 by our synthesized material and other recently reported materials [17,51–60]. In a previous study, UV irradiation was mostly used as the energy source to initiate the photocatalytic reduction of CO_2. The reductants, such as H_2 gas, and the electron donors, such as NaOH and $KHCO_3$, were also used to enhance the CO_2 reduction efficiency or selectivity. Therefore, the real application of the studies for industrial reduction of CO_2 is limited, because of high energy consumption and safety issues. In contrast, our synthesized Cu@V-TiO_2/PU materials showed a novel photocatalytic activity for the reduction of CO_2 to produce CO and CH_4, because only water vapor was used as the reductant and visible light as the energy source. Thus, our obtained results are expected to open a new era in the applications of photocatalysts for the reduction of CO_2 to produce valuable fuels.

4. Conclusion

In this study, Cu and V co-doped Cu@V-TiO_2/PU photocatalysts were synthesized for CO_2 conversion using visible light as the energy source and H_2O vapor as a reductant to produce valuable fuels. Both Cu and V defected into the TiO_2 lattice, leading to the formation of Ti^{3+} and oxygen vacancies in the lattice. However, as the ionic radius of V^{4+} is closer to that of Ti^{4+} than is that of Cu^{2+}, V^{4+} was doped into the TiO_2 lattice more effectively than

Cu^{2+}. The Ti^{3+} formed in the doped TiO_2 lattice created an intermediate band between the valence band and the conduction band of TiO_2, which increased the electron–hole pair separation efficiency of TiO_2 and enhanced the light absorption by the metal-doped TiO_2/PU. The oxygen vacancies existing on the surface of the photocatalyst induced new adsorption sites to adsorb CO_2, and the generated electrons and holes reduced the adsorbed CO_2 with H_2O vapor to produce CO and CH_4. The 2Cu@4V-TiO_2/PU photocatalyst, with Cu/TiO_2 and V/TiO_2 ratios of 2 and 4 wt.%, respectively, exhibited the highest rate of defection into the TiO_2 lattice, leading to the maximum formation of Ti^{3+} and oxygen vacancies with the highest reduction efficiency of the doped photocatalyst. The rates of CH_4 and CO production from the photocatalytic reduction of CO_2 with H_2O vapor by 2Cu@4V-TiO_2/PU under visible light were 933 and 588 μmol g^{-1} cat. h^{-1}, respectively. The synthesized photocatalysts generated sufficient electrons and holes for the reduction of CO_2. Therefore, CH_4 was selectively produced rather than CO.

Acknowledgments

This work was supported by the Korea Research Fellowship Program through the National Research Foundation of Korea (NRF) funded by the Ministry of Science, ICT and Future Planning (2015H1D3A1066572).

Appendix A. Supplementary material

Supplementary data associated with this article can be found, in the online version, at http://dx.doi.org/10.1016/j.jcat.2016.10.030.

References

[1] R. Gusain, P. Kumar, O.P. Sharma, S.L. Jain, O.P. Khatri, Reduced graphene oxide–CuO nanocomposites for photocatalytic conversion of CO_2 into methanol under visible light irradiation, Appl. Catal. B: Environ. 181 (2016) 352–362.
[2] P.N. Paulino, V.M.M. Salim, N.S. Resende, Zn-Cu promoted TiO_2 photocatalyst for CO_2 reduction with H_2O under UV light, Appl. Catal. B: Environ. 185 (2016) 362–370.
[3] M. Tahir, N.S. Amin, Performance analysis of nanostructured NiO–In_2O_3/TiO_2 catalyst for CO_2 photoreduction with H_2 in a monolith photoreactor, Chem. Eng. J. 285 (2016) 635–649.
[4] Y. Li, W.N. Wang, Z. Zhan, M.H. Woo, C.Y. Wu, P. Biswas, Photocatalytic reduction of CO_2 with H_2O on mesoporous silica supported Cu/TiO_2 catalysts, Appl. Catal. B: Environ. 100 (2010) 386–392.
[5] C.M. White, B.R. Strazisar, E.J. Granite, J.S. Hoffman, H.W. Pennline, Separation and capture of CO_2 from large stationary sources and sequestration in geological formations – coalbeds and deep saline aquifers, J. Air Waste Manage. Assoc. 53 (2003) 645–715.
[6] J. Low, B. Cheng, J. Yua, M. Jaroniec, Carbon-based two-dimensional layered materials for photocatalytic CO_2 reduction to solar fuels, Energy Storage Mater. 3 (2016) 24–25.
[7] T. Inoue, A. Fujishima, S. Konishi, K. Honda, Photoelectrocatalytic reduction of carbon dioxide in aqueous suspensions of semiconductor powers, Nature 277 (1979) 637–638.
[8] Y. Liu, S. Zhou, J. Li, Y. Wang, G. Jiang, Z. Zhao, B. Liu, X. Gong, A. Duan, J. Liu, Y. Wei, L. Zhang, Photocatalytic reduction of CO_2 with water vapor on surface La-modified TiO_2 nanoparticles with enhanced CH_4 selectivity, Appl. Catal. B: Environ. 168–169 (2015) 125–131.
[9] A. Tóth, G. Halasi, T. Bánsági, F. Solymosi, Reactions of propane with CO_2 over Au catalysts, J. Catal. 337 (2016) 57–64.
[10] Y. Wang, J. Zhao, T. Wang, Y. Li, X. Li, J. Yin, C. Wang, CO_2 photoreduction with H_2O vapor on highly dispersed CeO_2/TiO_2 catalysts: surface species and their reactivity, J. Catal. 337 (2016) 293–302.
[11] M. Wang, D. Wang, Z. Li, Self-assembly of CPO-27-Mg/TiO_2 nanocomposite with enhanced performance for photocatalytic CO_2 reduction, Appl. Catal. B: Environ. 183 (2016) 47–52.
[12] R. Jaiswal, N. Patel, A. Dashora, R. Fernandes, M. Yadav, R. Edla, R.S. Varma, D.C. Kothari, B.L. Ahuja, A. Miotello, Efficient Co-B-codoped TiO_2 photocatalyst for degradation of organic water pollutant under visible light, Appl. Catal. B: Environ. 183 (2016) 242–253.
[13] R. Jaiswal, J. Bharambe, N. Patel, A. Dashora, D.C. Kothari, A. Miotello, Copper and nitrogen co-doped TiO_2 photocatalyst with enhanced optical absorption and catalytic activity, Appl. Catal. B: Environ. 168–169 (2015) 333–341.
[14] T.D. Pham, B.K. Lee, The advanced removal of benzene from aerosols by photocatalytic oxidation and adsorption of Cu–TiO_2/PU under visible light irradiation, Appl. Catal. B: Environ. 182 (2016) 172–183.
[15] T.D. Pham, B.K. Lee, Novel adsorption and photocatalytic oxidation for removal of gaseous toluene by V-doped TiO_2/PU under visible light, J. Hazard. Mater. 300 (2015) 493–503.
[16] R. Amrollahi, M.S. Hamdy, G. Mul, Understanding promotion of photocatalytic activity of TiO_2 by Au nanoparticles, J. Catal. 319 (2014) 194–199.
[17] Z. Xiong, H. Wang, N. Xu, H. Li, B. Fang, Y. Zhao, J. Zhang, C. Zheng, Photocatalytic reduction of CO_2 on Pt^{2+}-Pt^0/TiO_2 nanoparticles under UV/Vis light irradiation: a combination of Pt^{2+} doping and Pt nanoparticles deposition, Int. J. Hydrogen Energy 40 (2015) 10049–10062.
[18] T.D. Pham, B.K. Lee, Cu doped TiO_2/GF for photocatalytic disinfection of *Escherichia coli* in bioaerosols under visible light irradiation: application and mechanism, Appl. Surf. Sci. 296 (2014) 15–23.
[19] T.D. Pham, B.K. Lee, Advanced removal of *C. famata* in bioaerosols by simultaneous adsorption and photocatalytic oxidation of Cu-doped TiO_2/PU under visible irradiation, Chem. Eng. J. 286 (2016) 377–386.
[20] S. Naraginti, T.V.L. Thejaswini, D. Prabhakaran, A. Sivakumar, V.S.V. Satyanarayana, A.S. Arun Prasad, Enhanced photo-catalytic activity of Sr and Ag co-doped TiO_2 nanoparticles for the degradation of Direct Green-6 and Reactive Blue-160 under UV & visible light, Spectrochim. Acta Part A: Mol., Biomol., Spectrosc. 149 (2015) 571–579.
[21] W.F. Chen, P. Koshy, C.C. Sorrell, Effect of intervalence charge transfer on photocatalytic performance of cobalt- and vanadium-codoped TiO_2 thin film, Int. J. Hydrogen Energy 40 (2015) 16215–16229.
[22] B. Benalioua, M. Mansour, A. Bentouami, B. Boury, E.H. Elandaloussi, The layered double hydroxide route to Bi–Zn co-doped TiO_2 with high photocatalytic activity under visible light, J. Hazard. Mater. 288 (2015) 158–167.
[23] M.M. Rodriguez, X.H. Peng, L.J. Liu, Y. Li, J.M. Andino, A density functional theory and experimental study of CO_2 interaction with brookite TiO_2, J. Phys. Chem. C 116 (2012) 19755–19764.
[24] T.D. Pham, B.K. Lee, Novel integrated approach of adsorption and photo-oxidation using Ag-TiO_2/PU for bioaerosol removal under visible light, Chem. Eng. J. 275 (2015) 357–365.
[25] L.F. Chiang, R. Doong, Cu–TiO_2 nanorods with enhanced ultraviolet- and visible-light photoactivity for bisphenol A degradation, J. Hazard. Mater. 277 (2014) 84–92.
[26] Y. Zou, S.Z. Kang, X. Li, L. Qin, J. Mu, TiO_2 nanosheets loaded with Cu: a low-cost efficient photocatalytic system for hydrogen evolution from water, Int. J. Hydrogen Energy 39 (2014) 15403–15410.
[27] E. Morrison, D. Gutiérrez-Tauste, C. Domingo, E. Vigil, J.A. Ayllón, One step room temperature photodeposition of Cu/TiO_2 composite films and its conversion to CuO/TiO_2, Thin Solid Films 517 (2009) 5621–5624.
[28] R. Jaiswal, N. Patel, D.C. Kothari, A. Miotello, Improved visible light photocatalytic activity of TiO_2 co-doped with vanadium and nitrogen, Appl. Catal. B: Environ. 126 (2012) 47–54.
[29] X. Yang, F. Ma, K. Li, Y. Guo, J. Hu, W. Li, M. Huo, Y. Guo, Mixed phase titania nanocomposite codoped with metallic silver and vanadium oxide: new efficient photocatalyst for dye degradation, J. Hazard. Mater. 175 (2010) 429–438.
[30] W. Cha, S. Chin, E. Park, S.T. Yun, J. Jurng, Photocatalytic performance of V_2O_5/TiO_2materials prepared by chemical vapor condensation and impregnation method under visible-light, Powder Technol. 258 (2014) 352–357.
[31] S. Klosek, D. Raftery, Visible light driven V-doped TiO_2 photocatalyst and its photooxidation of ethanol, J. Phys. Chem. B 105 (2002) 2815–2819.
[32] C. Gargori, S. Cerro, R. Galindo, A. Garcia, M. Llusar, J. Badenes, G. Monros, New vanadium doped calcium titanate ceramic pigment, Ceram. Int. 37 (2011) 3665–3670.
[33] M.S.P. Francisco, V.R. Mastelaro, Inhibition of the anatase-rutile phase transformation with addition of CeO_2 to CuO-TiO_2 system: Raman spectroscopy, X-ray diffraction, and textural studies, Chem. Mater. 14 (2002) 2514–2518.
[34] S.B. Yuan, P. Meriaudeau, V. Perrichon, Catalytic combustion of diesel soot particles on copper-catalysts supported on TiO_2 – effect of potassium promoter on the activity, Appl. Catal. B: Environ. 3 (1994) 319–333.
[35] F. Ren, H. Li, Y. Wang, J. Yang, Enhanced photocatalytic oxidation of propylene over V-doped TiO_2 photocatalyst: reaction mechanism between V^{5+} and single-electron-trapped oxygen vacancy, Appl. Catal. B: Environ. 176 (2015) 160–172.
[36] Y. Liu, L.C. Yan, R.Q. Hui, Z. Zhang, W.C. Yi, Effects of silver ion doping on the surface defect characteristics of TiO_2, Res. Chem. Intermed. 30 (2004) 569–577.
[37] M.M. Mohamed, M.S. Al-Sharif, Visible light assisted reduction of 4-nitrophenol to 4-aminophenol on Ag/TiO_2 photocatalysts synthesized by hybrid templates, Appl. Catal. B: Environ. 142–143 (2013) 432–441.
[38] T.D. Nguyen-Phan, M.B. Song, H. Yun, E.J. Kim, E.S. Oh, E.W. Shin, Characterization of vanadium-doped mesoporous titania and its adsorption of gaseous benzene, Appl. Surf. Sci. 257 (2011) 2024–2031.
[39] C.J. Lin, W.T. Yang, Ordered mesostructured Cu-doped TiO_2 spheres as active visible-light-driven photocatalysts for degradation of paracetamol, Chem. Eng. J. 237 (2014) 131–137.
[40] A. Kubacka, M.J. Munoz-Batista, M. Fernández-García, S. Obregón, G. Colón, Evolution of H_2 photoproduction with Cu content on CuO_x-TiO_2 composite catalysts prepared by a microemulsion method, Appl. Catal. B: Environ. 163 (2015) 214–222.

[41] M. Gurulakshmi, M. Selvaraj, A. Selvamani, P. Vijayan, N.R.S. Rekha, K. Shanthi, Enhanced visible-light photocatalytic activity of V_2O_5/S-TiO_2 nanocomposites, Appl. Catal. A: Gen. 449 (2012) 31–46.
[42] B. Wang, G. Zhang, X. Leng, Z. Sun, S. Zheng, Characterization and improved solar light activity of vanadium doped TiO_2/diatomite hybrid catalysts, J. Hazard. Mater. 284 (2015) 212–220.
[43] E.S. Aazam, Visible light photocatalytic degradation of thiophene using Ag–TiO_2/multi-walled carbon nanotubes nanocomposite, Ceram. Int. 40 (2014) 6705–6711.
[44] R. Jaiswal, J. Bharambe, R. Patel, A. Dashora, D.C. Kothari, A. Miotello, Copper and nitrogen co-doped TiO_2 photocatalyst with enhanced optical absorption and catalytic activity, Appl. Catal. B: Environ. 168–169 (2015) 333–341.
[45] Y. Zou, S.Z. Kang, X. Li, J. Qin, M. Mu, TiO_2 nanosheets loaded with Cu: a low-cost efficient photocatalytic system for hydrogen evolution from water, Int. J. Hydrogen Energy 39 (2014) 15403–15410.
[46] L. Laokiat, P. Khemthong, N. Grisdanurak, P. Sreearunothai, W. Pattanasiriwisawa, W. Klysubun, Photocatalytic degradation of benzene, toluene, ethylbenzene, and xylene (BTEX) using transition metal-doped titanium dioxide immobilized on fiberglass cloth, Korean J. Chem. Eng. 29 (2012) 377–383.
[47] J. Tauc, R. Grigorovici, A. Vancu, Optical properties and electronic structure of amorphous germanium, Phys. Status Solidi 15 (1996) 627–637.
[48] M. Hussain, N. Russo, G. Saracco, Photocatalytic abatement of VOCs by novel optimized TiO_2 nanoparticles, Chem. Eng. J. 166 (2011) 138–149.
[49] L. Liu, Y. Li, Understanding the reaction mechanism of photocatalytic reduction of CO_2 with H_2O on TiO_2-based photocatalysts: a review, Aerosol Air Quality Res. 14 (2014) 453–469.
[50] W. Pipornpong, R. Wanbayor, V. Ruangpornvisuti, Adsorption CO_2 on the perfect and oxygen vacancy defect surfaces of anatase TiO_2 and its photocatalytic mechanism of conversion to CO, Appl. Surf. Sci. 257 (2011) 10322–10328.
[51] M. Tahir, B. Tahir, Dynamic photocatalytic reduction of CO_2 to CO in a honeycomb monolith reactor loaded with Cu and N doped TiO_2 nanocatalysts, Appl. Surf. Sci. 377 (2016) 244–252.
[52] M. Tahir, B. Tahir, N.A.S. Amin, Gold-nanoparticle-modified TiO_2 nanowires for plasmon-enhanced photocatalytic CO_2 reduction with H_2 under visible light irradiation, Appl. Surf. Sci. 356 (2015) 1289–1299.
[53] S. Iguchi, Y. Hasegawa, K. Teramura, S. Hosokawa, T. Tanaka, Preparation of transition metal-containing layered double hydroxides and application to the photocatalytic conversion of CO_2 in water, J. CO_2 Util. 15 (2016) 6–14.
[54] Y. Wei, J. Jiao, Z. Zhao, J. Liu, J. Li, G. Jiang, Y. Wang, A. Duan, Fabrication of inverse opal TiO_2-supported Au@CdS core–shell nanoparticles for efficient photocatalytic CO_2 conversion, Appl. Catal. B: Environ. 179 (2015) 422–432.
[55] L. Ye, D. Wu, D.H. Chu, B. Wang, H. Xie, H.Y. Yip, P.K. Wong, Phosphorylation of g-C_3N_4 for enhanced photocatalytic CO_2 reduction, Chem. Eng. J. 304 (2016) 376–383.
[56] M. Jiang, Y. Gao, Z. Wang, Z. Ding, Photocatalytic CO_2 reduction promoted by a $CuCo_2O_4$ cocatalyst with homogeneous and heterogeneous light harvesters, Appl. Catal. B: Environ. 198 (2016) 180–188.
[57] J. Ding, Y. Bu, M. Ou, Y. Yu, Q. Zhong, M. Fan, Facile decoration of carbon fibers with Ag nanoparticles for adsorption and photocatalytic reduction of CO_2, Appl. Catal. B: Environ. 202 (2017) 314–325.
[58] B. Pan, S. Luo, W. Su, X. Wang, Photocatalytic CO_2 reduction with H_2O over $LaPO_4$ nanorods deposited with Pt cocatalyst, Appl. Catal. B: Environ. 168–169 (2015) 458–464.
[59] B. Tahir, M. Tahir, N.S. Amin, Gold–indium modified TiO_2 nanocatalysts for photocatalytic CO_2 reduction with H_2 as reductant in a monolith photoreactor, Appl. Surf. Sci. 338 (2015) 1–14.
[60] Y. He, Y. Wang, L. Zhang, B. Teng, M. Fan, High-efficiency conversion of CO_2 to fuel over ZnO/g-C_3N_4 photocatalyst, Appl. Catal. B: Environ. 168–169 (2015) 1–8.